Monthly Notices
of the
ROYAL ASTRONOMICAL SOCIETY

Mon. Not. R. Astron. Soc. **423,** 1766–1774 (2012) doi:10.1111/j.1365-2966.2012.20997.x

# Searching for a CU Virginis-type cyclotron maser from $\sigma$ Orionis E: the role of the magnetic quadrupole component

P. Leto,[1]★ C. Trigilio,[1] C. S. Buemi,[1] F. Leone[2] and G. Umana[1]

[1]*INAF – Osservatorio Astrofisico di Catania, Via S. Sofia 78, 95123 Catania, Italy*
[2]*Università di Catania, Dipartimento di Fisica e Astronomia, Sezione Astrofisica, Via S. Sofia 78, 95123 Catania, Italy*

Accepted 2012 March 26. Received 2012 March 1; in original form 2011 November 15

**ABSTRACT**

In this paper, we present new and archive radio measurements obtained with the Very Large Array of the magnetic chemically peculiar (MCP) star $\sigma$ Orionis E. The radio data have been obtained at different frequencies and they are well distributed along the rotational phases. We analyse in detail the radio emission from $\sigma$ Ori E with the aim of finding evidence for circularly polarized radio pulses. Up to now, among MCP stars, only CU Virginis has shown 100 per cent polarized time-stable radio pulses, explained as highly directive electron cyclotron maser emission, visible from Earth at particular rotational phases, like a pulsar. Our analysis shows that there is no hint of coherent emission at frequencies below 15 GHz. We conclude that the presence of a quadrupolar component of the magnetic field, dominant within few stellar radii from the star, where the maser emission should be generated, inhibits the onset of the cyclotron maser instability in $\sigma$ Ori E.

**Key words:** masers – stars: chemically peculiar – stars: individual: $\sigma$ Orionis E – stars: magnetic field – radio continuum: stars.

## 1 INTRODUCTION

Magnetic chemically peculiar (MCP) stars present photometric, spectroscopic and magnetic variability with a single period. As for the magnetic field, the most important observable is the effective or longitudinal magnetic field ($B_e$), which is the average over the stellar visible disc of the longitudinal components of the magnetic field (Leone, Catalano & Catanzaro 2000). To explain the previous phenomenology, Babcock (1949) and Stibbs (1950) proposed the presence of a magnetic dipole, whose axis is tilted with respect to the rotational axis (the so-called oblique rotator model), and a non-uniform distribution of some chemical elements on the stellar surface, which rotates rigidly. Spectral, light and magnetic variability would be a consequence of stellar rotation. Later, it was found that MCP stars can present multipolar magnetic fields. Bychkov, Bychkova & Madej (2005) have collected all available MCP magnetic curves, and they have shown that, in many cases, their shapes are more complex than a simple sinusoidal wave.

Non-thermal radio emission is observed from about 25 per cent of MCP stars (Leone, Trigilio & Umana 1994). In agreement with the oblique rotator model, the radio emission is also variable as a consequence of the stellar rotation (Leone 1991). This suggests that the radio emission arises from a stable optically thick corotating magnetosphere. Radio emission is ascribed to a radiatively driven stellar wind. The gas flow breaks the magnetic field lines far from the star (Alfvén surface) forming current sheets, where electrons are accelerated to the mildly relativistic regime. Energetic electrons propagate back, along thin magnetospheric layers called the the middle magnetosphere, to the inner magnetospheric regions, radiating by the gyrosynchrotron emission mechanism at radio wavelengths (Trigilio et al. 2004; Leto et al. 2006).

Of the MCP stars, CU Virginis (HD 124224 = HR 5313) is the only known source characterized by broad-band, highly polarized and time-stable pulses at 1.4 and 2.5 GHz (Trigilio et al. 2000, 2008, 2011; Ravi et al. 2010; Lo et al. 2012). Stevens & George (2010) have also reported a pulse detection at 610 MHz. Radio pulses stand out for 1 dex over the continuous emission, and the single pulse duration ranges from 5 to 10 per cent of the rotational period. The radio pulses are observed in coincidence with the null values of $B_e$, which is when the magnetic dipole axis is perpendicular to the line of sight.

Such behaviour has been ascribed to the electron cyclotron maser (ECM) emission mechanism powered by an anisotropic pitch-angle (the angle between electron velocity and local magnetic field) distribution that the non-thermal electrons, responsible of the gyrosynchrotron stellar radio emission, can develop when propagating in a magnetic flux tube towards regions of increasing magnetic field strength. Electrons with an initial large pitch angle are soon reflected outwards because of the magnetic mirroring, whereas electrons with a small pitch angle can reach the inner magnetospheric layers where they are thermalized in the dense plasma. The reflected electron

★E-mail: pleto@oact.inaf.it

population is characterized by a pitch-angle distribution not found for electrons with a small pitch angle. This mechanism amplifies the extraordinary magneto-ionic mode, producing nearly 100 per cent circularly polarized radiation at frequencies very close to the first or second harmonic of the local gyrofrequency ($\nu_B = 2.8 \times 10^{-3} B$/G GHz), in a direction almost perpendicular to the local magnetic field lines (Melrose & Dulk 1982). However, the fundamental harmonic is probably suppressed by the gyromagnetic absorption.

It is considered that the ECM mechanism accounts for the strongly polarized, intense and narrow-band short time spikes observed in the Sun (Willson 1985; Winglee & Dulk 1986), dMe flare stars (Lang et al. 1983; Lang & Willson 1988; Abada-Simon et al. 1994, 1997) and RS CVn binaries (Slee, Haynes & Wright 1984; Osten et al. 2004). The ECM explains planetary low-frequency emission, in particular the decametric radiation of Jupiter and the Earth's auroral kilometric radiation (AKR; Treumann 2006).

The fully polarized pulses observed on CU Vir are broad-band and persistent over a long time-scale (yr). The large bandwidth is a consequence of the wide range of the magnetic field strength in the region where the maser amplification occurs. The observed maser emission is the superimposition of narrow-band emission from different rings above the magnetic poles. The continuous supply of non-thermal electrons, developing a loss-cone anisotropy, keeps the ECM emission stable. Following the tangent plane beaming model, proposed for the AKR (Mutel, Christopher & Pickett 2008) and successfully applied to explain the narrow peaks observed on CU Vir (Trigilio et al. 2011), the amplified radiation is beamed tangentially to the polar ring where the cyclotron maser instability takes place. Then, during the propagation through the denser magnetized plasma of the inner magnetosphere, the radiation is refracted upward by a few degrees (Trigilio et al. 2011; Lo et al. 2012). Because the magnitude of this angle depends on the frequency, the radiation is detected at different moments during the rotation of the star, causing a frequency drift of the observed pulses.

Highly polarized broad-band radio pulses, still explained as ECM, have also been recognized in ultra-cool main-sequence dwarf stars (Berger et al. 2001; Burgasser & Putman 2005; Hallinan et al. 2006, 2007, 2008). Despite the great difference between the physical characteristics of these two extreme classes of stars, late M-type and MCP stars show similar behaviour at radio wavelengths. The existence of a well-ordered and stable axisymmetric magnetic field in rapidly rotating fully convective M-type stars (Donati et al. 2006a, 2008; Morin et al. 2008a,b) could be the reason for the observed similarity.

The study of radio pulses from CU Vir has also made it possible to find evidence of variations in the stellar rotational period with a high degree of confidence (Trigilio et al. 2008, 2011). The discovery of CU Vir-type coherent emission in other MCP stars would be a useful tool for the study of the angular momentum evolution in this type of star.

On the basis of the results gathered from CU Vir, to make it possible to observe the same type of coherent emission from other MCP stars, an appropriate stellar magnetic field geometry is needed, with $B_e$ presenting at least a null value during the stellar rotation. Among the already known MCP stars presenting radio emission, $\sigma$ Orionis E (HD 37479 = HR 1932) is an ideal candidate to search for the presence of this type of coherent emission. Its magnetic field presents the appropriate geometry, with the rotation axis inclination $i = 72^\circ$ and magnetic axis obliquity $\beta = 56^\circ$ (Bohlender et al. 1987).

The coherent pulses have been observed from CU Vir ($B_p$ = 3000 G; Trigilio et al. 2000) at low frequencies (<2.5 GHz). We expect that ECM emission from $\sigma$ Ori E could be observed at higher frequencies, as a consequence of the stronger magnetic field ($B_p$ = 6800 G; Trigilio et al. 2004). In this paper, we present new multifrequency (1.4, 5, 8.4, 15, 22 and 43 GHz) Very Large Array (VLA)[1] observations of $\sigma$ Ori E. In addition, in order to obtain radio light curves that are as complete as possible, we have retrieved all unpublished VLA archive data. The primary aim is to search for amplified strongly polarized emission, but we can also probe different layers of the magnetosphere of $\sigma$ Ori E, because of the dependence of the frequency of the gyrosynchrotron radio emission on the magnetic field strength.

## 2 σ ORI E

$\sigma$ Ori E is a magnetic helium-strong star of spectral type B2V, with mass $M_* = 8.9\ M_\odot$ (Hunger, Heber & Groote 1989) and radius $R_* = 4.2\ R_\odot$ (Shore & Brown 1990), located at a distance of about 350 pc (ESA 1997). It is significantly hotter than CU Vir (spectral type A0V), which involves a stronger radiatively driven wind, and therefore a greater mass-loss rate. However, the polar magnetic field strength of $\sigma$ Ori E is 6800 G, versus 3000 G for CU Vir, and the rotational period is 1.19 d versus 0.52 d. Both these factors influence the confinement of the wind, meaning that the two stars have similar magnetospheres, both with an Alfvén radius of about 15 $R_*$ (Trigilio et al. 2004; Leto et al. 2006). This reinforces our decision to search for evidence of CU Vir-type coherent emission from $\sigma$ Ori E.

The long history of the photometric, spectroscopic and magnetic variability presented by $\sigma$ Ori E is documented in the catalogue of observed periods for AP stars by Catalano & Renson (1984), and its supplements (Catalano & Renson 1988; Catalano, Renson & Leone 1991a, 1993). Townsend et al. (2010) have concluded that $\sigma$ Ori E is spinning down because of the magnetic braking. They have supplied the ephemeris

$$\mathrm{HJD} = 244\,2778.829 + 1.1908229E + 1.44 \times 10^{-9} E^2 \quad \mathrm{(d)},$$

referring to the deeper light minimum. The spin-down of $\sigma$ Ori E has already been theoretically predicted by magnetohydrodynamics simulations (Ud-Doula, Owocky & Townsend 2009).

The global magnetic field of $\sigma$ Ori E has been steady over three decades (Oksala et al. 2011), and a pure magnetic dipole has been assumed since the study of Landstreet & Borra (1978). Fig. 1 shows the magnetic field measurements of $\sigma$ Ori E by Landstreet & Borra (1978), Bohlender et al. (1987) and Oksala et al. (2011), phased with the previous ephemeris. A data fit with a single wave equation,

$$B_e = B_0 + B_1 \sin 2\pi(\Phi - \Phi_0),$$

gives a reduced $\chi^2 = 12.4$. Here, $B_0 = 0.55 \pm 0.02$ kG, $B_1 = 2.24 \pm 0.03$ kG and $\Phi_0 = 0.478 \pm 0.002$.

For a long time it has been known that the variability of MCP stars can be accurately modelled through a sinusoidal wave and its first harmonic (Catalano, Kroll & Leone 1991b). Indeed, a fit of magnetic data with the equation:

$$B_e = B_0 + B_1 \sin 2\pi(\Phi - \Phi_0) + B_2 \sin 2\pi(2\Phi - \Phi_1)$$

results in a reduced $\chi^2 = 1.6$, suggesting the non-dipolar nature of the $\sigma$ Ori E magnetic field. Here $B_0 = 0.62 \pm 0.02$ kG, $B_1 = 2.21 \pm 0.03$ kG, $B_2 = 0.63 \pm 0.03$ kG, $\Phi_0 = 0.473 \pm 0.002$ and $\Phi_1 = 0.563 \pm 0.007$.

[1] The VLA is a facility of the National Radio Astronomy Observatory, which is operated by Associated Universities, Inc. under cooperative agreement with the National Science Foundation.

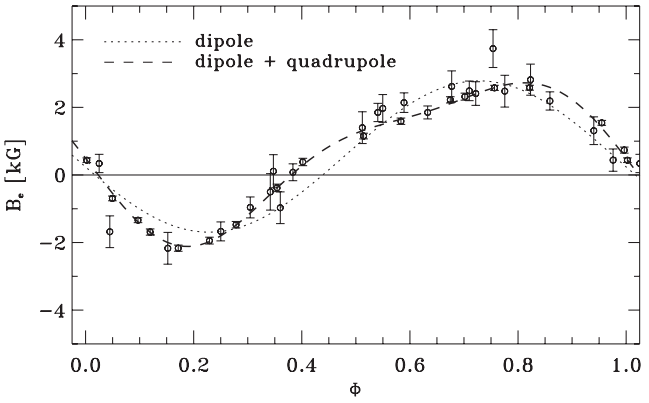


**Figure 1.** The open circles show the fit of the magnetic field measurements from the literature. The dotted line is the single wave fit and the dashed line is the double wave fit. The solid horizontal line coincides with the null effective surface magnetic field.

Landolfi, Bagnulo & Landi Degl'Innocenti (1998) have shown that the $B_e$ variation as a result of a pure quadrupole is about 10 per cent of the variability resulting from a dipole of equal polar strength. This means that $\sigma$ Ori E would present a quadrupole component at least two times stronger than the dipole component.

The presence of multipolar magnetic components in $\sigma$ Ori E is proved by the asymmetric emission features on the H$\alpha$ wings. These periodically variable features have been ascribed to two circumstellar plasma clouds trapped in the magnetosphere and corotating with the star (Landstreet & Borra 1978); the trapped material was also recognized from ultraviolet observations (Smith & Groote 2001). To explain why one of the two features is stronger than the other, Groote & Hunger (1982) suggested an asymmetry in the two clouds. In the case of $\delta$ Ori C, an MCP star twin of $\sigma$ Ori E, which also presents similar asymmetric emission features on the H$\alpha$ wings, Leone et al. (2010) mapped the circumstellar matter distribution and ascribed the asymmetry between the two clouds to the magnetic quadrupole component necessary to explain the Stokes $V$ profiles of the spectral lines.

We conclude that the phenomenology of $\sigma$ Ori E cannot be modelled as a simple dipole and that higher-order components are necessary to explain the observational data.

## 3 RADIO OBSERVATIONS AND DATA REDUCTION

Multifrequency observations of $\sigma$ Ori E were carried out with the VLA in different epochs. Table 1 reports the instrumental and observational details for each data set.

**Table 1.** VLA observing log.

| Code | Frequency (GHz) | Epoch | Conf. | Flux cal. | Phase cal. |
|---|---|---|---|---|---|
| AL346 | 5/15/43 | 95-Apr | D | 3C48 | 0541−056 |
| AT233 | 1.4/5 | 99-Oct | AB | 3C48 | 0541−056 |
| AL568 | 8.4/15 | 02-May | AB | 3C286 | 0541−056 |
| AL618 | 5/15/22/43 | 04-Jan | BC | 3C286 | 0541−056 |
| Archive VLA data | | | | | |
| AL267 | 5/8.4/15 | 92-Oct | A | 3C286 | 0541−056 |
| AL348 | 5/8.4/15/22/43 | 95-Mar | D | 3C286 | 0532+075 |
| AL372 | 5/8.4/15 | 96-Mar | C | 3C48 | 0541−056 |

To avoid significant phase fluctuations, the scans on $\sigma$ Ori E were shorter than the coherence time of Earth's atmosphere and they were embedded between phase calibrator measurements. The 22- and 43-GHz observations were carried out using the fast switching mode between the source and phase calibrator.

The data were calibrated and mapped using the standard procedures of the Astronomical Image Processing System (AIPS). The flux density for the Stokes $I$ parameter was obtained by fitting a two-dimensional Gaussian (JMFIT) at the source position in the cleaned maps, integrated over contiguous scans; the integration time ranges from about 10 min to about 1 h. As for the uncertainty in the flux-density measurements, we assume the rms of the map.

The fraction of the circularly polarized flux density (Stokes $V$ parameter) was instead determined by performing a direct Fourier transform of the visibilities at the source position (DFTPL) without any temporal average. We are justified in using this procedure by the absence of other circularly polarized sources in the field. The Stokes $V$ parameters were later averaged with the same integration time as for Stokes $I$. All VLA measurements are listed in Table 2.

## 4 RADIO PROPERTIES OF $\sigma$ ORI E

### 4.1 Light curves

Fig. 2 shows the radio flux versus the rotational phase for $\nu \leq 15$ GHz. For completeness, we also plot the measurements from the literature at 5 GHz (Drake et al. 1987; Leone & Umana 1993). The top panel shows the variability of $B_e$ (Landstreet & Borra 1978; Bohlender et al. 1987; Oksala et al. 2011).

As is already known (Leone 1991; Leone & Umana 1993; Trigilio et al. 2004), the light curve at 5 GHz of $\sigma$ Ori E is characterized by the presence of two maxima associated with the extrema of the magnetic field. We observe a similar modulation in the flux curve at 1.4 GHz. At both 1.4 and 5 GHz, the minima in the light curves are close in phase with the null magnetic field, which occurs when the axis of the dipole is perpendicular to the line of sight.

The shapes of the light curves at 8.4 and 15 GHz are more complex, and any relation with the $B_e$ variability is no longer simple. At 8.4 GHz, more than two maxima are detected, two of which are clearly associated with the two maxima observed at $\Phi \approx 0.3$ and 0.95 in the 15-GHz light curve. The amplitude of the light curves increases with the frequency, ranging from about 49 per cent (at 1.4 GHz) to about 82 per cent (at 15 GHz) of the median.

With the aim to detect CU Vir-type pulses in $\sigma$ Ori E, we focus our attention on the phase windows where we expect to see them. These windows are around the rotational phases corresponding to the null of the magnetic-field curve. The first null is at $\Phi \approx 0.9$–0.1 and the second is at $\Phi \approx 0.3$–0.5, both with a duration $\Delta\Phi_{\rm null} \approx 0.2$. The phase coverage of the radio measurements around the first null is almost continuous in the frequency range 1.4–15 GHz, while around the second null there are fewer data. Assuming that a pulse extends over a phase window $\Delta\Phi_{\rm ECM} \approx 0.05$, as for the narrowest pulse observed in CU Vir, we estimate that the probability of missing an ECM pulse in the first null is zero, because the maximum phase gap $\Delta\Phi_{\rm gap}$ between contiguous points is smaller than $\Delta\Phi_{\rm ECM}$ for all the observed frequencies. In contrast, around the second null, there are several gaps for which $\Delta\Phi_{\rm gap} > \Delta\Phi_{\rm ECM}$. In this case, we estimate the probability of missing the ECM pulse as $(\Delta\Phi_{\rm gap} - \Delta\Phi_{\rm ECM})/\Delta\Phi_{\rm null}$. Considering all the gaps in this phase window, these probabilities are 63, 25, 16 and 14 per cent at 1.5, 5, 8.4 and 15 GHz, respectively. However, for the whole rotational period, we obtain 13, 5, 12 and 15 per cent.

**Table 2.** New and archival VLA observations.

| JD 240 0000+ | $S_I$ ($S_V$) (mJy) | σ (mJy) | JD 240 0000+ | $S_I$ ($S_V$) (mJy) | σ (mJy) | JD 240 0000+ | $S_I$ ($S_V$) (mJy) | σ (mJy) | JD 240 0000+ | $S_I$ ($S_V$) (mJy) | σ (mJy) | JD 240 0000+ | $S_I$ ($S_V$) (mJy) | σ (mJy) |
|---|---|---|---|---|---|---|---|---|---|---|---|---|---|---|
| | $\nu = 1.4$ GHz | | 50171.677[d] | 4.10(−0.03) | 0.07 | 51461.958[e] | 4.42(+0.13) | 0.05 | 50171.629[d] | 3.78(−0.27) | 0.05 | 49827.591[c] | 4.50(+0.10) | 0.40 |
| 51453.833[e] | 2.60(+0.10) | 0.15 | 50172.377[d] | 4.10(+0.30) | 0.10 | 51461.982[e] | 4.14(+0.20) | 0.06 | 50171.688[d] | 4.27(−0.14) | 0.06 | 49833.434[c] | 3.30(−0.40) | 0.30 |
| 51453.862[e] | 2.50(+0.10) | 0.15 | 50172.437[d] | 3.43(+0.22) | 0.08 | 51462.009[e] | 4.14(+0.15) | 0.06 | 50172.448[d] | 3.38(+0.43) | 0.06 | 49837.382[c] | 4.10(+0.10) | 0.30 |
| 51453.896[e] | 2.10(+0.00) | 0.15 | 50172.496[d] | 3.14(+0.05) | 0.08 | 51462.037[e] | 4.21(+0.35) | 0.06 | 50172.507[d] | 3.23(+0.29) | 0.06 | 50170.358[d] | 3.20(−0.30) | 0.10 |
| 51453.951[e] | 2.00(+0.00) | 0.20 | 50172.555[d] | 3.44(+0.04) | 0.08 | 51462.061[e] | 4.00(+0.24) | 0.05 | 50172.567[d] | 3.99(+0.10) | 0.05 | 50170.418[d] | 3.40(−0.30) | 0.10 |
| 51453.998[e] | 1.70(+0.10) | 0.20 | 50172.615[d] | 3.31(−0.01) | 0.07 | 51462.085[e] | 3.88(+0.15) | 0.06 | 50172.626[d] | 4.27(+0.05) | 0.05 | 50170.477[d] | 3.10(−0.30) | 0.10 |
| 51454.050[e] | 1.80(−0.10) | 0.20 | 50172.674[d] | 3.44(+0.08) | 0.07 | 51462.111[e] | 3.53(+0.27) | 0.05 | 50172.685[d] | 4.36(+0.04) | 0.06 | 50170.537[d] | 3.80(−0.40) | 0.10 |
| 51454.135[e] | 2.30(+0.00) | 0.20 | 51453.831[e] | 3.10(+0.10) | 0.10 | 53031.789[g] | 3.40(+0.05) | 0.08 | 52417.192[f] | 3.10(+0.50) | 0.20 | 50170.596[d] | 5.20(−0.40) | 0.10 |
| 51455.827[e] | 2.00(−0.10) | 0.15 | 51453.855[e] | 3.20(+0.20) | 0.20 | | $\nu = 8.4$ GHz | | 52417.200[f] | 2.80(+0.70) | 0.20 | 50170.655[d] | 5.60(−0.20) | 0.10 |
| 51455.862[e] | 2.30(+0.10) | 0.10 | 51453.878[e] | 3.10(+0.10) | 0.10 | 48906.869[a] | 4.40(+0.10) | 0.10 | 52417.208[f] | 2.80(+0.30) | 0.20 | 50170.707[d] | 5.80(−0.20) | 0.20 |
| 51455.902[e] | 2.40(+0.00) | 0.10 | 51453.902[e] | 3.40(+0.10) | 0.10 | 48906.887[a] | 4.40(+0.00) | 0.10 | 52417.217[f] | 3.20(+0.30) | 0.20 | 50171.411[d] | 3.70(+0.20) | 0.10 |
| 51455.941[e] | 2.80(−0.10) | 0.10 | 51453.934[e] | 3.11(−0.02) | 0.08 | 48906.901[a] | 4.20(−0.30) | 0.10 | 52417.227[f] | 2.80(+0.60) | 0.20 | 50171.470[d] | 4.40(+0.00) | 0.10 |
| 51455.998[e] | 2.70(+0.10) | 0.10 | 51453.957[e] | 3.09(+0.11) | 0.07 | 48906.915[a] | 4.00(−0.10) | 0.10 | 52417.238[f] | 2.80(+0.30) | 0.20 | 50171.530[d] | 4.10(+0.00) | 0.10 |
| 51456.067[e] | 2.70(+0.10) | 0.10 | 51453.981[e] | 3.16(+0.13) | 0.07 | 48906.934[a] | 3.90(−0.20) | 0.10 | 52417.250[f] | 2.50(+0.20) | 0.20 | 50171.589[d] | 3.90(−0.30) | 0.10 |
| 51456.120[e] | 2.70(+0.00) | 0.10 | 51454.004[e] | 3.12(+0.01) | 0.06 | 48907.011[a] | 4.30(−0.20) | 0.10 | 52417.262[f] | 2.50(+0.30) | 0.10 | 50171.648[d] | 3.50(−0.40) | 0.10 |
| 51456.162[e] | 2.80(+0.00) | 0.10 | 51454.032[e] | 3.25(−0.07) | 0.05 | 48907.030[a] | 4.60(−0.10) | 0.10 | 52417.276[f] | 2.80(+0.20) | 0.10 | 50171.700[d] | 3.90(−0.80) | 0.20 |
| 51458.841[e] | 2.00(−0.10) | 0.08 | 51454.060[e] | 3.28(−0.05) | 0.06 | 48907.048[a] | 4.70(−0.10) | 0.10 | 52417.291[f] | 3.10(+0.10) | 0.10 | 50172.408[d] | 4.00(+0.80) | 0.20 |
| 51458.899[e] | 2.20(+0.00) | 0.10 | 51454.083[e] | 3.22(+0.01) | 0.06 | 48907.067[a] | 4.80(+0.00) | 0.10 | 52417.306[f] | 3.60(+0.00) | 0.10 | 50172.467[d] | 3.20(+0.20) | 0.20 |
| 51458.956[e] | 2.30(−0.06) | 0.07 | 51454.107[e] | 3.44(−0.05) | 0.06 | 48907.086[a] | 4.90(+0.20) | 0.10 | 52417.321[f] | 3.60(−0.20) | 0.10 | 50172.527[d] | 3.20(+0.20) | 0.10 |
| 51459.031[e] | 2.60(+0.04) | 0.08 | 51454.130[e] | 3.78(+0.00) | 0.06 | 48907.163[a] | 5.00(+0.10) | 0.10 | 52417.337[f] | 3.90(+0.10) | 0.10 | 50172.586[d] | 4.80(−0.10) | 0.10 |
| 51459.122[e] | 2.40(+0.02) | 0.08 | 51454.154[e] | 3.96(−0.04) | 0.07 | 48908.854[a] | 3.90(+0.20) | 0.10 | 52417.352[f] | 4.00(+0.00) | 0.10 | 50172.645[d] | 5.10(+0.10) | 0.10 |
| 51461.929[e] | 2.70(+0.00) | 0.10 | 51454.176[e] | 3.87(−0.13) | 0.08 | 48908.873[a] | 3.70(+0.10) | 0.10 | 52417.367[f] | 3.70(−0.10) | 0.10 | 50172.697[d] | 5.80(−0.10) | 0.20 |
| 51461.976[e] | 2.80(+0.20) | 0.10 | 51455.821[e] | 3.30(+0.20) | 0.10 | 48908.891[a] | 3.50(+0.40) | 0.10 | 52417.383[f] | 3.73(−0.06) | 0.08 | 52417.229[f] | 3.30(+0.70) | 0.15 |
| 51462.021[e] | 2.80(+0.10) | 0.10 | 51455.845[e] | 3.41(+0.15) | 0.08 | 48908.910[a] | 3.30(+0.20) | 0.10 | 52417.398[f] | 3.70(+0.10) | 0.10 | 52417.284[f] | 2.90(+0.40) | 0.20 |
| 51462.067[e] | 2.80(+0.00) | 0.10 | 51455.868[e] | 3.75(+0.01) | 0.08 | 48908.929[a] | 3.20(+0.40) | 0.10 | 52417.413[f] | 4.00(−0.10) | 0.10 | 52417.315[f] | 3.20(+0.00) | 0.15 |
| | $\nu = 5$ GHz | | 51455.892[e] | 3.80(+0.20) | 0.10 | 48909.006[a] | 2.80(+0.20) | 0.10 | 52417.428[f] | 3.90(−0.10) | 0.10 | 52417.345[f] | 3.90(+0.10) | 0.15 |
| 48906.821[a] | 3.20(+0.00) | 0.10 | 51455.923[e] | 4.03(+0.18) | 0.08 | 48909.024[a] | 2.80(+0.20) | 0.10 | 52417.444[f] | 4.00(+0.00) | 0.10 | 52417.376[f] | 4.50(−0.40) | 0.15 |
| 48906.973[a] | 4.10(+0.20) | 0.10 | 51455.947[e] | 4.13(+0.14) | 0.08 | 48909.043[a] | 3.00(+0.10) | 0.10 | 52417.459[f] | 4.10(−0.10) | 0.10 | 52417.406[f] | 5.20(+0.50) | 0.15 |
| 48907.125[a] | 4.90(−0.10) | 0.10 | 51455.971[e] | 4.04(+0.18) | 0.07 | 48909.062[a] | 2.70(+0.20) | 0.10 | 52417.473[f] | 4.00(−0.10) | 0.10 | 52417.437[f] | 5.00(+0.00) | 0.15 |
| 48908.816[a] | 4.70(+0.20) | 0.10 | 51455.994[e] | 4.09(+0.15) | 0.08 | 48909.081[a] | 3.50(+0.00) | 0.10 | 52417.484[f] | 4.00(+0.00) | 0.10 | 52417.477[f] | 3.90(−0.10) | 0.20 |
| 48908.968[a] | 3.20(+0.00) | 0.10 | 51456.022[e] | 3.71(+0.17) | 0.08 | 48909.157[a] | 3.80(+0.00) | 0.10 | 52417.496[f] | 4.40(−0.10) | 0.10 | 52417.519[f] | 3.60(−0.30) | 0.20 |
| 48909.119[a] | 3.40(+0.10) | 0.10 | 51456.050[e] | 3.49(+0.26) | 0.07 | 48910.867[a] | 3.80(+0.00) | 0.10 | 52417.506[f] | 3.90(−0.20) | 0.20 | 53031.748[f] | 2.50(+0.30) | 0.20 |
| 48910.811[a] | 3.30(+0.00) | 0.15 | 51456.073[e] | 3.42(+0.33) | 0.07 | 48910.886[a] | 3.77(−0.05) | 0.08 | 52417.515[f] | 3.90(+0.00) | 0.20 | 53031.800[f] | 3.50(+0.50) | 0.20 |
| 48910.962[a] | 3.60(+0.10) | 0.15 | 51456.097[e] | 3.81(+0.20) | 0.08 | 48910.905[a] | 3.46(+0.03) | 0.08 | 52417.523[f] | 3.70(+0.00) | 0.20 | | $\nu = 22$ GHz | |
| 48911.114[a] | 4.30(+0.20) | 0.15 | 51456.120[e] | 3.32(+0.06) | 0.08 | 48910.924[a] | 3.73(−0.11) | 0.08 | 52417.531[f] | 3.90(+0.10) | 0.20 | 49803.407[b] | 2.70(+0.10) | 0.30 |
| 49803.498[b] | 3.00(−0.20) | 0.20 | 51456.144[e] | 3.55(+0.17) | 0.08 | 48911.000[a] | 4.30(+0.10) | 0.10 | | $\nu = 15$ GHz | | 49803.452[b] | 3.50(−0.60) | 0.30 |
| 49803.647[b] | 3.80(−0.40) | 0.20 | 51458.818[e] | 2.84(−0.01) | 0.08 | 48911.019[a] | 4.00(+0.10) | 0.10 | 48906.841[a] | 4.90(−0.10) | 0.30 | 49803.513[b] | 4.20(+0.50) | 0.30 |
| 49827.591[c] | 4.50(+0.10) | 0.10 | 51458.841[e] | 3.24(+0.06) | 0.07 | 48911.038[a] | 3.80(+0.00) | 0.10 | 48906.993[a] | 3.40(−0.70) | 0.40 | 49803.557[b] | 3.30(+0.50) | 0.20 |
| 49833.450[c] | 4.30(−0.10) | 0.10 | 51458.865[e] | 3.59(+0.06) | 0.07 | 48911.057[a] | 3.50(+0.30) | 0.10 | 48907.145[a] | 5.30(−0.40) | 0.40 | 49803.602[b] | 2.90(−0.60) | 0.30 |
| 49837.398[c] | 3.00(+0.00) | 0.10 | 51458.889[e] | 3.73(−0.07) | 0.07 | 48911.075[a] | 3.80(+0.10) | 0.10 | 48908.836[a] | 3.40(+0.90) | 0.40 | 53031.777[g] | 3.20(+0.60) | 0.10 |
| 50170.328[d] | 3.30(+0.00) | 0.10 | 51458.920[e] | 3.96(−0.10) | 0.08 | 49803.487[b] | 3.55(+0.00) | 0.10 | 48908.988[a] | 3.20(+0.90) | 0.40 | 53031.828[g] | 4.60(+0.00) | 0.10 |
| 50170.387[d] | 3.97(−0.04) | 0.08 | 51458.944[e] | 4.05(−0.06) | 0.07 | 49803.636[b] | 3.60(−0.20) | 0.10 | 48909.139[a] | 5.20(+0.50) | 0.40 | 53031.859[g] | 5.30(+0.20) | 0.10 |
| 50170.446[d] | 4.05(−0.10) | 0.08 | 51458.967[e] | 4.11(−0.16) | 0.07 | 50170.398[d] | 3.84(−0.16) | 0.06 | 48910.831[a] | 3.50(−0.20) | 0.40 | | $\nu = 43$ GHz | |
| 50170.506[d] | 3.93(−0.02) | 0.07 | 51458.991[e] | 4.46(−0.11) | 0.07 | 50170.458[d] | 3.50(−0.10) | 0.20 | 48910.982[a] | 4.40(+0.10) | 0.40 | 49803.542[b] | 3.60(−0.20) | 0.40 |
| 50170.565[d] | 4.28(−0.08) | 0.07 | 51459.019[e] | 4.59(−0.10) | 0.06 | 50170.517[d] | 4.12(−0.13) | 0.05 | 48911.134[a] | 3.00(+1.00) | 0.40 | 49819.488[c] | 3.10(+0.70) | 0.80 |
| 50170.624[d] | 4.19(−0.02) | 0.08 | 51459.046[e] | 4.95(+0.03) | 0.06 | 50170.576[d] | 4.84(−0.07) | 0.05 | 49803.385[b] | 2.50(+0.10) | 0.30 | 49833.453[c] | 2.00(+0.20) | 0.90 |
| 50170.684[d] | 3.78(−0.06) | 0.08 | 51459.070[e] | 4.98(−0.06) | 0.06 | 50170.636[d] | 4.69(−0.06) | 0.06 | 49803.430[b] | 3.80(+0.00) | 0.25 | 49837.400[c] | 3.10(+0.90) | 0.90 |
| 50171.380[d] | 3.14(+0.03) | 0.08 | 51459.094[e] | 4.60(−0.15) | 0.07 | 50170.695[d] | 4.56(−0.14) | 0.06 | 49803.475[b] | 4.30(+0.60) | 0.25 | 53031.763[g] | 2.60(+0.60) | 0.20 |
| 50171.439[d] | 2.90(+0.02) | 0.08 | 51459.117[e] | 4.97(−0.08) | 0.07 | 50171.391[d] | 3.57(−0.02) | 0.06 | 49803.535[b] | 4.20(−0.10) | 0.30 | 53031.814[g] | 3.00(+0.20) | 0.30 |
| 50171.499[d] | 3.14(−0.02) | 0.07 | 51459.141[e] | 4.52(+0.04) | 0.07 | 50171.451[d] | 3.56(+0.09) | 0.06 | 49803.580[b] | 3.40(−0.20) | 0.25 | 53031.843[g] | 4.20(+0.60) | 0.30 |
| 50171.558[d] | 3.55(+0.03) | 0.08 | 51459.163[e] | 3.60(+0.00) | 0.10 | 50171.510[d] | 4.03(−0.03) | 0.06 | 49803.624[b] | 3.20(−0.30) | 0.25 | | | |
| 50171.617[d] | 4.00(−0.06) | 0.08 | 51461.935[e] | 4.18(+0.20) | 0.06 | 50171.570[d] | 3.74(−0.10) | 0.06 | 49820.603[c] | 6.00(−0.60) | 0.30 | | | |

Notes. [a] AL267. [b] AL348. [c] AL346. [d] AL372. [e] AT233. [f] AL568. [g] AL618.

### 4.2 Radio spectrum

The 22- and 43-GHz VLA measurements of σ Ori E do not cover the whole rotational period. However, our 22- and 43-GHz observations agree with the steep flux increment observed at 15 GHz ($\Phi \approx 0.95$). We can then trace the complete radio spectrum from 1.4 to 43 GHz in the range of phases, 0.9–1, when the flux at 15 GHz approximately doubles. To minimize the effect of the lack of simultaneity of higher-frequency measurements, we have fixed the phases, $\Phi = 0.867$, 0.910, 0.922, 0.934 and 0.998, coinciding with the measurements at 43 GHz and with the interpolated value between the two closest in phases 43-GHz observations. Fluxes at other frequencies have been obtained by fits of the light curves (see Fig. 3, left panels). The five spectra are labelled (a)–(e) in Fig. 3.

The radio spectrum (a), obtained before the rising phase of the 15-GHz flux, peaks at intermediate frequencies (5–8.4 GHz). The radio spectra (b), (c) and (d) just before the 15-GHz maximum instead peak at a higher frequency (15 GHz) and show a steep rise at 43 GHz (Fig. 3, top-right panel). At frequencies below 15 GHz, the spectral index is positive, with $\alpha \approx 0.3$ ($S_\nu \propto \nu^\alpha$). The spectrum (e), obtained after the maximum, closely resembles the spectrum (d) (having a similar 15-GHz flux level but obtained before the maximum) at the lowest frequencies, whereas at the highest frequencies (22 and 43 GHz) the fluxes are decreasing.

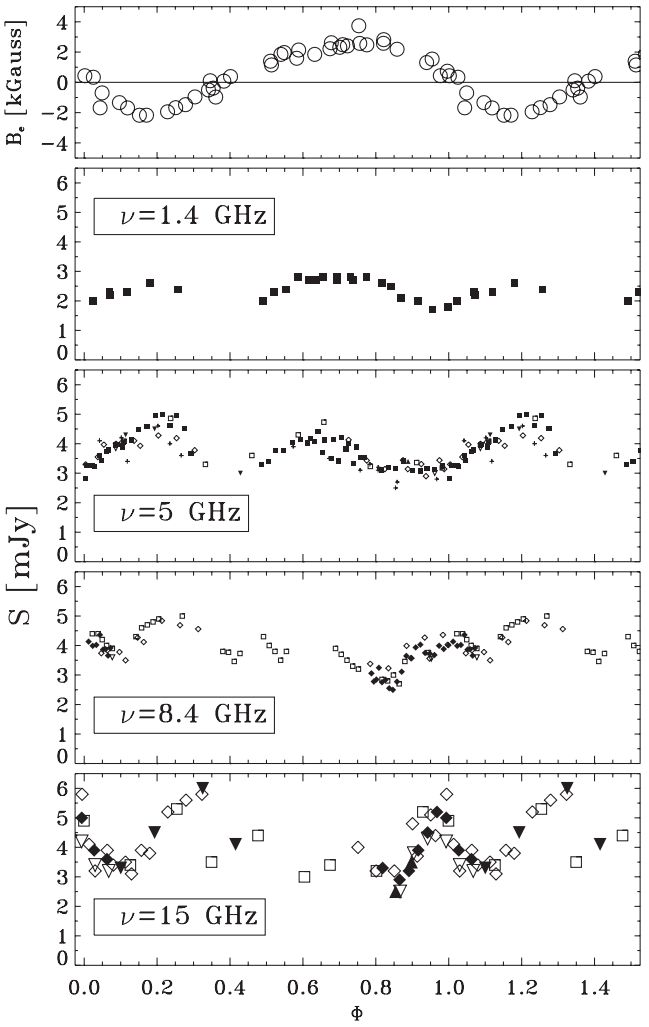


**Figure 2.** VLA measurements of $\sigma$ Ori E plotted versus the rotation phase $\Phi$: AL267 (□), AL348 (▽), AL346 (▼), AL372 (◇), AT233 (■), AL568 (◆) and AL618 (▲). The data from the literature at 5 GHz are indicated by +. The symbol size is equal to the flux error. The top panel shows the magnetic field curve from the literature.

### 4.3 Circular polarization

The circularly polarized radio emission shows two extrema of opposite signs (Fig. 4, bottom panels), detected above the $3\sigma$ detection threshold, associated with the magnetic field extrema (Fig. 1). The degree of polarization enhances as the frequency increases. A positive degree of circular polarization is detected when the north magnetic pole is close to the line of sight, and it is negative in the presence of the south pole. When the magnetic poles are close to the direction of the line of sight, we observe most of the radially oriented field lines. In this case, the gyrosynchrotron mechanism gives rise to partially polarized radio emission – right hand for the north pole and left hand for the south pole.

The overall behaviour of the circularly polarized radiation from $\sigma$ Ori E closely resembles the case of CU Vir at 5, 8.4 and 15 GHz (Leto et al. 2006). This can be considered the typical behaviour of gyrosynchrotron emission from a magnetosphere characterized by a mainly dipolar symmetry.

## 5 EFFECT OF THE MAGNETIC QUADRUPOLE ON THE RADIO EMISSION

### 5.1 Comparison with the three-dimensional model

In order to investigate the radio emission from MCP stars, in Trigilio et al. (2004) we developed a three-dimensional (3D) model to compute the gyrosynchrotron emission from a magnetosphere shaped in the framework of the oblique rotator model, assuming a simple magnetic dipole. Leto et al. (2006) extended the 3D model to solve the radiation transfer for the circularly polarized emission (Stokes $V$ parameter). Such a 3D modelling has been successfully applied to $\sigma$ Ori E and HD 37017 by Trigilio et al. (2004) and to CU Vir by Leto et al. (2006).

In this model, a radiatively driven stellar wind flows along the magnetic field lines. The wind channelled by the magnetic field reaches the magnetic equator. At the Alfvén radius, where the kinetic energy density of the wind exceeds the magnetic one, the stellar wind breaks the magnetic field lines generating the current sheets, where particle acceleration occurs. The energetic electrons moving towards the stellar surface emit by the gyrosynchrotron mechanism. This thin layer is called the middle magnetosphere and it is connected to the annular regions around the magnetic poles at high magnetic latitudes. At lower magnetic latitudes, the wind is instead confined in a dead zone (inner magnetosphere), resulting in an accumulation of circumstellar matter whose density decreases outwards, in agreement with the magnetically confined wind shock model (Babel & Montmerle 1997). This circumstellar material absorbs the continuous gyrosynchrotron radiation, resulting in the observed deep rotational modulation.

Here, we adopt the model parameters given by Trigilio et al. (2004), used to fit the 5-GHz light curve of $\sigma$ Ori E found in the literature, to compute the expected radio flux density and the fraction of circular polarization ($\pi_c = S_V/S_I$) for all the frequencies. In Fig. 4, we compare the simulations with the observations. The 1.4-GHz Stokes $I$ variability is reproduced in shape, but slightly overestimating the average flux. As for the highest frequencies, our 3D model fails to reproduce the observed Stokes $I$ variability. In contrast, the Stokes $V$ simulations are in good agreement with the measurements.

Because the source is optically thick, the radiation at different frequencies probes the stellar magnetosphere at different depths, where $\tau \approx 1$. Higher frequencies are mainly emitted in the inner regions, where the magnetic field is stronger. In particular, by inspecting the modelled radio maps of $\sigma$ Ori E shown by Trigilio et al. (2004), the bulk of the 5-GHz gyrosynchrotron emission is found to arise from the magnetospheric regions 3–8 $R_*$ away from the stellar surface, whereas that at 15 GHz originates from the inner layers (1–5 $R_*$).

We conclude that the 3D model reproduces the behaviour of the 1.4- and 5-GHz radio emission, coming mainly from regions far from the star, where the dipolar component of the magnetic field dominates. The nearly dipolar symmetry can also be identified from the behaviour of the polarized emission, reproduced well by the model simulations at all the frequencies (Fig. 4, bottom panels). At 8.4 and 15 GHz, the model fails to reproduce the observed Stokes $I$ modulation, as expected if a non-dipolar magnetic field component is present.

In the case of the gyrosynchrotron mechanism, the radio emission from a region with almost parallel magnetic field lines, directed towards us (north) or in the opposite direction (south), is right-hand or left-hand circularly polarized (RCP or LCP); Stokes $V$, which

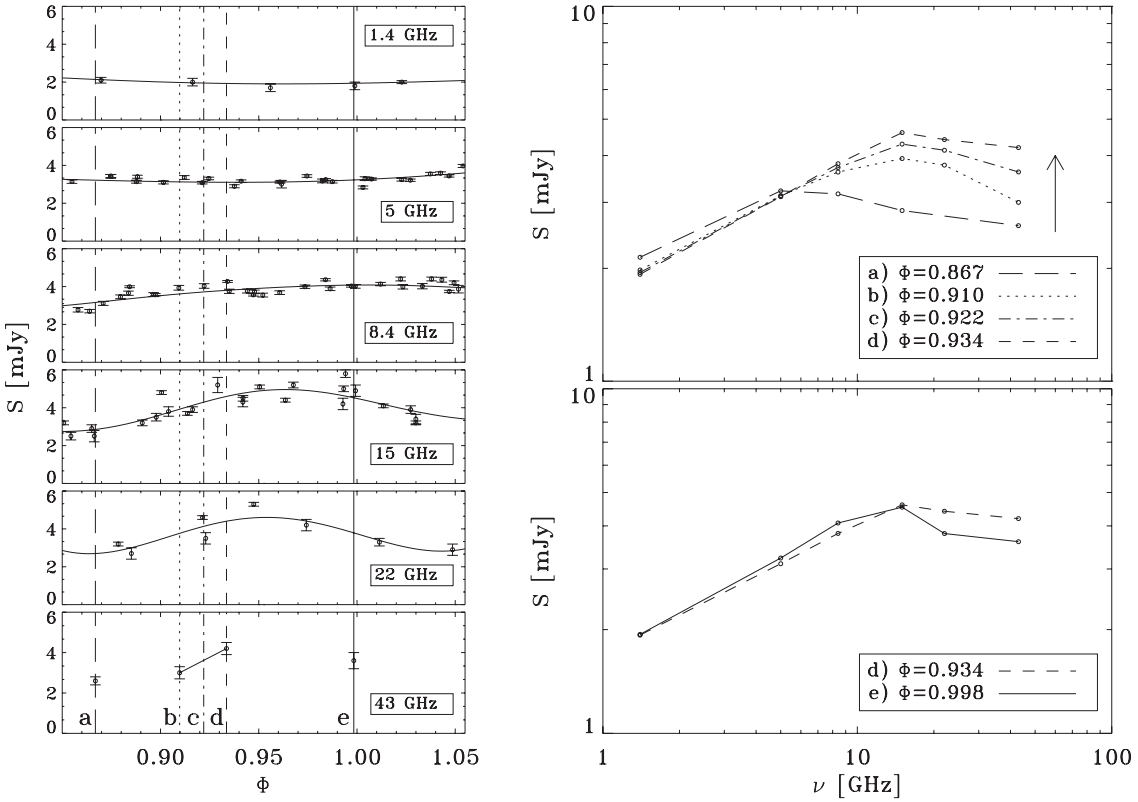


**Figure 3.** Left panels: zoom of the radio light curves at phases where high-frequency data are available; the vertical lines (a, b, c, d, e) show the phases where the spectra have been realized. Right panels: radio spectra at phases (a)–(e); the upper panel shows the rising phase and the lower panel shows the decay phase.

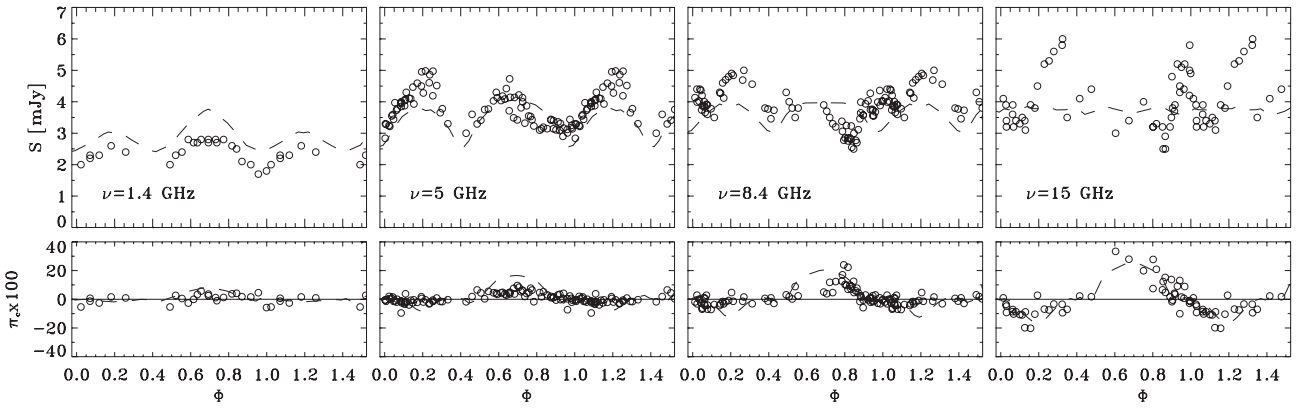


**Figure 4.** Comparison of the observed radio light curves of $\sigma$ Ori E and the theoretical curves (dashed line) computed with the 3D model of Trigilio et al. (2004).

is the difference between RCP and LCP, is positive or negative, whereas Stokes $I$, which is the sum of RCP and LCP, is sensitive to both polarizations. In a region with a dis-homogeneous magnetic field on a small scale, the polarization is, on average, null. When a quadrupolar field is present, we always see regions with antiparallel field lines; Stokes $V$ is always null, while Stokes $I$ depends on the strength of each individual component. In this simple way, we can explain both the behaviour of Stokes $V$, which agrees well with the dipolar model at any frequency, and the behaviour of the low-frequency Stokes $I$, arising from regions where only the dipolar field is relevant. The high-frequency Stokes $I$ is sensitive to the quadrupolar component, which is important in the low magnetosphere. We are supported in such a conclusion by the Stokes $I$ and $V$ variability presented at 5 GHz by HR 5624 (Lim, Drake & Linsky 1996), which is characterized by a multipolar magnetic field (Landstreet 1990).

The spectra shown in Fig. 3 show that the radio flux density at higher frequencies rises steeply, rising to a maximum at phase $\approx$0.95, as is clearly observed in the 15-GHz light curve. This could be a consequence of strong dis-homogeneity in the magnetic field close to the star.

### 5.2 Absence of the cyclotron maser

In this work, we mainly aim to find CU Vir-like pulses from $\sigma$ Ori E. In the following, we compute the expected frequency range of the ECM in our target.

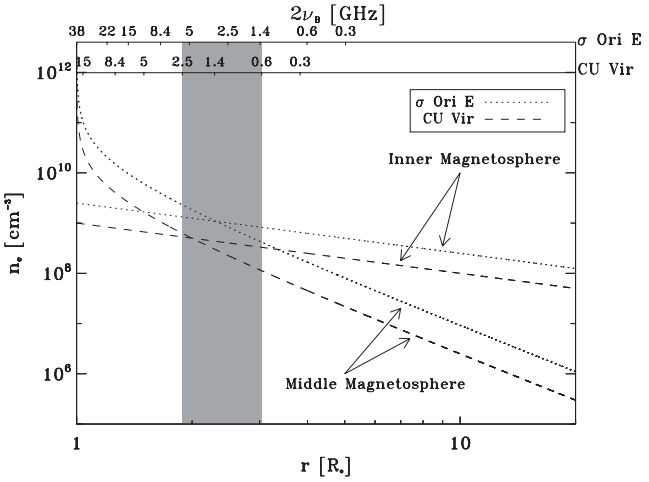


**Figure 5.** Radial dependence of the thermal electron density number inside the middle and inner magnetosphere, for $\sigma$ Ori E and CU Vir. On the top $x$-axis, the ECM frequencies ($2\nu_B$) for the two stars are shown. The shaded area identifies the corresponding magnetospheric regions.

The minimum maser frequency observed in CU Vir is 610 MHz (Stevens & George 2010) and the maximum is 2.5 GHz. Because the maser frequency is a harmonic of the local gyrofrequency, $\nu = s \times \nu_B$, with $s = 2$. Assuming a simple dipolar field, for which the magnetic field strength above the pole is given by

$$B_{\rm dip} = B_{\rm p}({\rm R}_*/R)^3,$$

we can deduce that for CU Vir ($B_{\rm p} = 3000$ G) the maser at 610 MHz is generated at $2\,{\rm R}_*$ above the stellar surface. The shaded area of Fig. 5 defines the frequencies and the corresponding distances associated with the ECM pulses, as observed for CU Vir. At the same height, for $\sigma$ Ori E, with a polar field strength $B_{\rm p} = 6800$ G, the corresponding frequency of emission is 1.4 GHz. Therefore, the cyclotron maser emission from $\sigma$ Ori E, if it does exist, should be observable at frequencies higher than 1.4 GHz. The maximum possible frequency is given by the second harmonic of the gyrofrequency very close to the stellar surface, corresponding to about 38 GHz.

Moreover, a necessary condition for the ECM is that the local plasma frequency must be lower than the local gyrofrequency (i.e. $\nu_{\rm p} \ll \nu_{\rm B}$; Melrose & Dulk 1982). Because the plasma frequency is given by $\nu_{\rm p} = 9 \times 10^{-6} n_{\rm e}^{1/2}$ GHz, the maser emission near to the magnetic pole is possible only if the local thermal electron number density is less than about $4 \times 10^{12}\,{\rm cm}^{-3}$. In the current model, the thin cavity where the maser should originate is the middle magnetosphere above the magnetic pole, where the local plasma is the ionized thermal wind that flows along the magnetic field lines. Following Trigilio et al. (2008), and adopting the characteristic values of the wind derived with the 3D model for $\sigma$ Ori E (Trigilio et al. 2004), we estimate that the density of the wind is about $10^{11}\,{\rm cm}^{-3}$ near the stellar surface, well below the theoretical quenching limit. As the magnetic field strength decreases going outwards, the plasma frequency equates the gyrofrequency at approximately 7 $R_*$ above the surface. Therefore, we can conclude that the condition for generation of the cyclotron maser is satisfied in the middle magnetosphere of $\sigma$ Ori E.

Fig. 5 shows the radial behaviour of the plasma density in the middle and inner magnetosphere for $\sigma$ Ori E (Trigilio et al. 2004) and CU Vir (Leto et al. 2006). As has recently been observed for CU Vir (Trigilio et al. 2011; Lo et al. 2012), the ray path of the ECM, which is polarized in the $x$-mode, is refracted by the plasma trapped in the inner magnetosphere. The refractive index is given by $n_{\rm refr} \approx \sqrt{1 - \nu_{\rm p}^2/2\nu_{\rm B}^2}$, with $\nu_{\rm ECM} \approx 2\nu_{\rm B}$. Because the conditions of the plasma are similar for $\sigma$ Ori E and CU Vir (Fig. 5), we expect an upwards refraction. In other words, the radiation should be deviated, not absorbed.

Despite the fact that the light curves in the expected frequency range of the ECM (between 1.4 and 15 GHz) are well sampled, in particular near the rotational phases where we expect to detect it (i.e. in coincidence with at least one null of the magnetic curve; Fig. 2), we do not see any hint of the pulses as observed for CU Vir. Because the frequencies of 1.4 and 15 GHz correspond to the second harmonic of the local gyrofrequency at 2 and 0.4 $R_*$ above the pole, respectively, we can conclude that, in this region, the conditions needed to trigger the cyclotron maser are not fulfilled.

As highlighted in this paper, the magnetic field of $\sigma$ Ori E is characterized by the presence of a quadrupolar component, whose strength $B_{\rm quad}$, which prevails on the stellar surface, decreases faster than the dipolar component ($B_{\rm quad} \propto R^{-5}$, $B_{\rm dip} \propto R^{-3}$). Therefore, the actual magnetic vector in the low magnetosphere can be quite different from the simple dipolar magnetic vector. As already discussed, this quadrupolar component significantly affects the gyrosynchrotron emission at a high frequency, originating in the deep magnetospheric layers. In a similar way, the quadrupolar component of the magnetic field, which is stronger than the dipolar component at a low altitude, affects the propagation of the electrons moving towards the stellar surface. This causes the magnetic mirroring point to move up, and consequently it causes a different interaction with the thermal plasma of the stellar magnetosphere and a possible change in the ECM conditions. In fact, for a charged particle moving with a pitch angle $\phi$ in a non-uniform magnetic field, its magnetic moment is invariant (i.e. $\sin^2\phi/B$ = constant), leading to magnetic mirroring when the particle moves in a converging magnetic field. Assuming a simple dipolar field for $\sigma$ Ori E, a non-thermal electron injected with $\phi_0 \approx 1^\circ$ at the Alfvén radius ($R_{\rm Alfvén} \approx 15\,R_*$), where $B_{\rm Alfvén} \approx 2$ G, will reach the stellar surface with a pitch angle $\phi \approx 90^\circ$ ($\sin^2\phi = \sin^2\phi_0 \times B_{\rm p}/B_{\rm Alfvén}$). If there is a magnetic quadrupolar component, which is two or three times stronger than the strength of the dipolar field, the same electron is reflected at 0.3–0.35 $R_*$ from the surface, and it cannot reach the deeper and denser magnetospheric layers; in this case, it is reflected back without being absorbed. Only those electrons injected at $R_{\rm Alfvén}$ with a very small pitch angle ($\ll 1^\circ$) can reach the stellar surface. Accordingly, the fraction of non-thermal electrons that can develop an anisotropic pitch-angle distribution is very small. Then, the loss-cone angle is already closed when the electrons reach the region where the maser at a frequency below 15 GHz should arise. The quadrupole component vanishes 5–6 $R_*$ away from the surface, and this explains the observed behaviour of $\sigma$ Ori E.

## 6 CAN O-TYPE STARS EMIT ECM PULSES?

Hot O-type stars have strong ionized stellar winds and, in a few cases, organized magnetic fields (Donati et al. 2002, 2006b), like MCP stars. Such characteristics imply that magnetic O-type stars might be sources of ECM.

Typically, MCP stars have weak winds ($\dot{M} \approx 10^{-10}$–$10^{-9}$ ${\rm M}_\odot$ ${\rm yr}^{-1}$) strongly dominated by magnetic fields ($B_{\rm p} \approx 1$–10 kG), with large corotating magnetospheres. The measured magnetic field in O-type stars is about 1 kG or less (Hubrig et al. 2011) and the mass-loss rate is higher than $10^{-7}$ ${\rm M}_\odot$ ${\rm yr}^{-1}$. Because $R_{\rm Alfvén} \propto B_{\rm p}^{1/2}/\dot{M}^{1/4}$

(Ud-Doula et al. 2009), the very massive wind and the relatively weak magnetic field locates the Alfvén surface of the known magnetic O-type stars close to the stellar surface ($<2\,R_*$). In the case of single magnetic O-type stars, shocks originating in the wind channelled by the magnetic field can accelerate electrons up to a relativistic energy (Van Loo, Runacres & Blomme 2006). In turn, these could emit at the radio regime by the gyrosynchrotron mechanism. However, O-type stars are characterized by radio emission at centimetre wavelengths mainly ascribed to the thermal free–free emission from the ionized stellar wind, whose typical spectral index is $\alpha \approx 0.6$ ($S_\nu \propto \nu^\alpha$; Wright & Barlow 1975). The radio photosphere, at centimetre wavelengths, has a radius of $\approx 100\,R_*$ (Blomme 2011), meaning that the plasma of the wind is optically thick inside and that any non-thermal emission generated within is completely absorbed (Van Loo et al. 2006). The ECM from O-type stars, if any, would suffer from the same absorption effect.

Moreover, for a main-sequence magnetic O-type star with stellar radius $R_* = 7$–$8\,\mathrm{R}_\odot$, radiative wind mass-loss rate $\dot{M} = 10^{-6}\,\mathrm{M}_\odot\ \mathrm{yr}^{-1}$, terminal velocity $v_\infty = 2000\ \mathrm{km\ s}^{-1}$ and dipolar magnetic field with $B_\mathrm{p} = 1000\,\mathrm{G}$, the condition $\nu_\mathrm{p} > \nu_\mathrm{B}$ is valid everywhere. This is further proof against the possibility that a magnetic O-type star can emit ECM pulse. Up to now, the signatures of the non-thermal emission mechanism – a flat or negative spectral index and variability – in O-type stars have only been observed in multiple systems. Thus, the origin of relativistic electrons has been ascribed to the acceleration in the shocks that take place in the colliding winds far from the stellar surface (Blomme 2011).

In conclusion, the conditions for generation and propagation of the ECM emission are not satisfied for the known magnetic O-type stars. The behaviour of the magnetized O-type stars is thus significantly different from that of MCP stars (B/A spectral type) in the radio domain. The key to explaining when the transition occurs is probably the shaping of the stellar magnetosphere, which depends on the mass-loss rate, the magnetic field strength and the rotational period.

## 7 CONCLUSIONS AND OUTLOOK

Up to now, CU Vir has been the only known MCP star presenting ECM emission. The characteristics of the MCP star $\sigma$ Ori E suggest that it should present the same phenomenology as CU Vir at frequencies higher than 1.4 GHz. We have obtained multifrequency radio observations during the whole of the rotation period of $\sigma$ Ori E, in particular at the phases where the ECM is expected. However, no cyclotron maser emission has been detected in this star.

There are indications that the magnetic field topology of $\sigma$ Ori E cannot be considered as a simple dipole. The presence of the quadrupole field could inhibit the development of the conditions able to power the cyclotron maser emission. Nevertheless, we cannot rule out the possibility that the ECM could occur at other frequencies not analysed in this paper, such as 2.5 GHz, or at phases near the second null of the magnetic curve, which are not fully covered.

However, in order to better understand the ECM in the wider context of plasma processes, it would be extremely interesting to extend such an investigation to a larger sample of MCP stars. The average radio luminosity of MCP stars is about $10^{16.8\pm0.9}$ erg s$^{-1}$ Hz$^{-1}$ (Drake et al. 1987; Linsky, Drake & Bastian 1992). It has also been shown that the radio luminosity of MCP stars increases with effective temperature (Linsky et al. 1992; Leone et al. 1994). The new-generation radio interferometers, such as the EVLA or the forthcoming Australian SKA Pathfinder (ASKAP), which will operate at 1.4 GHz, will allow us to reach a detection limit of a few μJy in all-sky deep surveys. Assuming a threshold of 10 μJy, we estimate to about 2000 pc the maximum distance within which it will be possible to detect radio emission from MCP stars. Following Renson & Manfroid (2009), we can assume that MCP stars are uniformly distributed in space. It is reasonable to expect that the number of radio detections will increase by about an order of magnitude, giving us an opportunity to obtain larger statistics of the physical conditions of the magnetospheres, such as the magnetic field strength and orientation and the thermal plasma density, to correlate with the ECM.

We would like to stress here that this class of objects provides a unique possibility to study the plasma process in stable magnetic structures, whose topologies are often well determined by several independent diagnostics (Bychkov et al. 2005). Thus, we can overcome the variability of the magnetic field, which is one of the major problems preventing accurate modelling of the ECM in very active stars, such dMe stars or close binary systems. However, considering earlier spectral types, stronger and denser stellar winds, together with a weaker magnetic field, should inhibit the onset of ECM instability. Moreover, as shown for the prototype CU Vir, observations of the persistent coherent pulses of ECM, which act like a clock for the star, in other MCP stars could be a valuable tool for studying the angular momentum evolution of objects belonging to this class.

## ACKNOWLEDGMENTS

We thank Mary Oksala for providing the magnetic field data, and the referee for constructive criticism which enabled us to improve this paper.

## REFERENCES

Abada Simon M., Lecacheux A., Louarn P., Dulk G. A., Belkora L., Bookbinder J. A., Rosolen C., 1994, A&A, 288, 219
Abada Simon M., Lecacheux A., Aubier M., Bookbinder J. A., 1997, A&A, 321, 841
Babcock H. W., 1949, Observatory, 69, 191
Babel J., Montmerle T., 1997, A&A, 323, 121
Berger E. et al., 2001, Nat, 410, 338
Blomme R., 2011, Bull. Soc. R. Sci. Liège, 80, 67
Bohlender D. A., Landstreet J. D., Brown D. N., Thompson I. B., 1987, ApJ, 323, 325
Burgasser A. J., Putman M. E., 2005, ApJ, 626, 486
Bychkov V. D., Bychkova L. V., Madej J., 2005, A&A, 430, 1143
Catalano F. A., Renson P., 1984, A&AS, 55, 371
Catalano F. A., Renson P., 1988, A&AS, 72, 1
Catalano F. A., Renson P., Leone F., 1991a, A&AS, 87, 59
Catalano F. A., Kroll R., Leone F., 1991b, A&A, 248, 179
Catalano F. A., Renson P., Leone F., 1993, A&AS, 98, 269
Donati J.-F., Babel J., Harries T. J., Howarth I. D., Petit P., Semel M., 2002, MNRAS, 333, 55
Donati J.-F., Forveille T., Collier Cameron A., Barnes J. R., Delfosse X., Jardine M. M., Valenti J. A., 2006a, Sci, 311, 633
Donati J.-F., Howarth I. D., Bouret J.-C., Petit P., Catala C., Landstreet J., 2006b, MNRAS, 365, L6
Donati J.-F. et al., 2008, MNRAS, 390, 545
Drake S. A., Abbot D. C., Bastian T. S., Bieging J. H., Churchwell E., Dulk G., Linsky J. L., 1987, ApJ, 322, 902
ESA, 1997, The *Hipparcos* and *Tycho* Catalogues, ESA SP-1200
Groote D., Hunger K., 1982, A&A, 116, 64
Hallinan G., Antonova A., Doyle J. G., Bourke S., Brisken W. F., Golden A., 2006, ApJ, 653, 690
Hallinan G. et al., 2007, ApJ, 663, L25

Hallinan G., Antonova A., Doyle J. G., Bourke S., Lane C., Golden A., 2008, ApJ, 684, 644
Hubrig S. et al., 2011, A&A, 528, 151
Hunger K., Heber U., Groote D., 1989, A&A, 224, 57
Landolfi M., Bagnulo S., Landi Degl'Innocenti M., 1998, A&A, 338, 111
Landstreet J. D., 1990, ApJ, 352, L5
Landstreet J. D., Borra E. F., 1978, ApJ, 224, L5
Lang K. R., Willson R. F., 1988, ApJ, 326, 300
Lang K. R., Bookbinder J., Golub L., Davis M. M., 1983, ApJ, 272, L15
Leone F., 1991, A&A, 252, 198
Leone F., Umana G., 1993, A&A, 268, 667
Leone F., Trigilio C., Umana G., 1994, A&A, 283, 908
Leone F., Catalano F. A., Catanzaro G., 2000, A&A, 355, 315
Leone F., Bohlender D. A., Bolton C. T., Buemi C., Catanzaro G., Hill G. M., Stift M. J., 2010, MNRAS, 401, 2739
Leto P., Trigilio C., Buemi C. S., Umana G., Leone F., 2006, A&A, 458, 831
Lim J., Drake S. A., Linsky J. L., 1996, in Taylor A. R., Paredes J. M., eds, ASP Conf. Ser. Vol. 93, Radio Emission from the Stars and the Sun. Astron. Soc. Pac., San Francisco, p. 324
Linsky J. L., Drake S. A., Bastian S. A., 1992, ApJ, 393, 341
Lo K. K. et al., 2012, MNRAS, 421, 3316
Melrose D. B., Dulk G. A., 1982, ApJ, 259, 844
Morin J. et al., 2008a, MNRAS, 384, 77
Morin J. et al., 2008b, MNRAS, 390, 567
Mutel R. L., Christopher I. W., Pickett J. S., 2008, Geophys. Res. Lett., 35, L07104
Oksala M. E., Wade G. A., Townsend R. H. D., Kochukhov O., Owocki S. P., 2011, in Neiner C., Wade G., Meynet G., Peters G., eds, Proc. IAU Symp. 272, Active OB Stars: Structure, Evolution, Mass Loss and Critical Limits. Kluwer, Dordrecht, p. 124
Osten R. A. et al., 2004, ApJS, 153, 317
Ravi V., Hobbs G., Wickramasinghe D., Champion D. J., Keith M., 2010, MNRAS, 408, L99
Renson P., Manfroid J., 2009, A&A, 498, 961
Shore N. S., Brown N. B., 1990, ApJ, 365, 665
Slee O. B., Haynes R. F., Wright A. E., 1984, MNRAS, 208, 865
Smith M. A., Groote D., 2001, A&A, 372, 208
Stevens I. R., George S. J., 2010, in Martí J., Luque-Escamilla P. L., Combi J. A., eds, ASP Conf. Ser. Vol. 422, High Energy Phenomena in Massive Stars. Astron. Soc. Pac., San Francisco, p. 135
Stibbs D. W. N., 1950, MNRAS, 110, 395
Townsend R. H. D., Oksala M.E, Cohen D. H., Owocki S. P., ud-Doula A., 2010, ApJ, 714, L318
Treumann R. A., 2006, A&AR, 13, 229
Trigilio C., Leto P., Leone F., Umana G., Buemi C., 2000, A&A, 362, 281
Trigilio C., Leto P., Umana G., Leone F., Buemi C. S., 2004, A&A, 418, 593
Trigilio C., Leto P., Umana G., Buemi C. S., Leone F., 2008, MNRAS, 384, 1437
Trigilio C., Leto P., Umana G., Buemi C. S., Leone F., 2011, ApJ, 739, L10
Ud-Doula A., Owocki S. P., Townsend R. H. D., 2009, MNRAS, 392, 1022
Van Loo S., Runacres M. C., Blomme R., 2006, A&A, 452, 1011
Willson R. F., 1985, Solar Phys., 96, 199
Winglee R. M., Dulk G. A., 1986, ApJ, 310, 432
Wright A. E., Barlow M. J., 1975, MNRAS, 170, 41

This paper has been typeset from a TEX/LATEX file prepared by the author.